PHYSICAL REVIEW D **89,** 055010 (2014)

Quasifixed point scenarios and the Higgs mass in the E_6 inspired supersymmetric models

R. Nevzorov

Theory Department, ITEP, Moscow 117218, Russia
ARC Centre of Excellence for Particle Physics at the Terascale and CSSM, School of Chemistry and Physics, The University of Adelaide, Adelaide, South Australia 5005, Australia

(Received 4 October 2013; published 17 March 2014)

We analyze the two-loop renormalization group (RG) flow of the gauge and Yukawa couplings within the E_6 inspired supersymmetric models with extra $U(1)_N$ gauge symmetry under which right-handed neutrinos have zero charge. In these models, single discrete $\tilde{Z}_2^H$ symmetry forbids the tree-level flavor-changing transitions and the most dangerous baryon and lepton number violating operators. We consider two different scenarios A and B that involve extra matter beyond the minimal supersymmetric Standard Model contained in three and four $5 + \bar{5}$ representations of $SU(5)$, respectively, plus three $SU(5)$ singlets which carry $U(1)_N$ charges. In scenario A, the measured values of the $SU(2)_W$ and $U(1)_Y$ gauge couplings lie near the fixed points of the RG equations. In scenario B, the contribution of two-loop corrections spoils the unification of gauge couplings, resulting in the appearance of the Landau pole below the grand unification scale M_X. The solutions for the Yukawa couplings also approach the quasifixed points with increasing their values at the scale M_X. We calculate the two-loop upper bounds on the lightest Higgs boson mass in the vicinity of these quasifixed points and compare the results of our analysis with the corresponding ones in the next-to-minimal supersymmetric Standard Model. In all these cases, the theoretical restrictions on the Standard-Model-like Higgs boson mass are rather close to 125 GeV.

DOI: 10.1103/PhysRevD.89.055010 PACS numbers: 12.60.Jv, 12.60.Cn, 12.60.Fr, 14.80.Da

I. INTRODUCTION

The recent discovery of a Standard-Model-like Higgs state with a mass around ~125 GeV [1,2] is consistent with the supersymmetric (SUSY) extensions of the Standard Model (SM). Indeed, in the minimal supersymmetric Standard Model (MSSM), the mass of the lightest Higgs particle, which manifests itself in the interactions with gauge bosons and fermions as a SM-like Higgs boson, does not exceed 130–135 GeV. Although the MSSM is one of the most attractive and best studied extensions of the SM, it suffers from the μ problem: the superpotential of the MSSM contains one bilinear term $\mu H_d H_u$ which is present before SUSY is broken. Thus one would naturally expect the parameter μ to be of the order of the Planck scale $M_{\rm Pl}$. On the other hand, in order to get the correct pattern of electroweak symmetry breaking (EWSB), μ is required to be of the order of the EW scale.

An elegant solution of the μ problem naturally arises in the framework of E_6 inspired models. At high energies E_6 can be broken down to the rank-5 gauge group that leads to low-energy gauge symmetry with an additional $U(1)'$ factor in comparison to the SM. The remaining $U(1)'$ symmetry is a linear combination of $U(1)_\psi$ and $U(1)_\chi$:

$$U(1)' = U(1)_\chi \cos\theta + U(1)_\psi \sin\theta. \tag{1}$$

Two anomaly-free $U(1)_\psi$ and $U(1)_\chi$ symmetries are defined by $E_6 \to SO(10) \times U(1)_\psi$, $SO(10) \to SU(5) \times U(1)_\chi$. If $\theta \neq 0\,\text{or}\,\pi$, the extra $U(1)'$ gauge symmetry forbids an elementary μ term but allows an interaction of the extra SM singlet superfield S with the Higgs doublet supermultiplets H_d and H_u in the superpotential: $\lambda S H_d H_u$. At the TeV scale the scalar component of the SM singlet superfield S acquires a nonzero vacuum expectation value (VEV) breaking $U(1)'$, and an effective μ term of the required size is automatically generated.

Here we focus on the supersymmetric extension of the SM which is based on the low-energy SM gauge group together with an extra $U(1)_N$ gauge symmetry that corresponds to the angle $\theta = \arctan\sqrt{15}$ in Eq. (1). Only in this exceptional supersymmetric Standard Model (E_6SSM) [3,4] right-handed neutrinos do not participate in the gauge interactions. As a consequence, they may be superheavy, shedding light on the origin of the mass hierarchy in the lepton sector. Because right-handed neutrinos are allowed to have large masses, they may decay into final states with lepton number $L = \pm 1$, thereby creating a lepton asymmetry in the early Universe that subsequently gets converted into the observed baryon asymmetry through the EW phase transition [5].

To ensure that E_6SSM is anomaly-free, the particle spectrum in this extension of the SM is extended to fill out three complete 27-dimensional representations of the gauge group E_6. Each 27-plet contains one generation of ordinary matter; singlet fields S_i; up- and down-type Higgs doublets H_i^u and H_i^d, respectively; and charged $\pm 1/3$ colored exotics D_i and $\bar{D}_i$. The matter content and correctly

TABLE I. The $U(1)_Y$ and $U(1)_N$ charges of matter fields in the E_6 inspired SUSY models with extra $U(1)_N$ gauge symmetry.

	Q	u^c	d^c	L	e^c	N^c	S	H^u	H^d	D	$\bar{D}$
$\sqrt{\frac{5}{3}}Q_i^Y$	$\frac{1}{6}$	$-\frac{2}{3}$	$\frac{1}{3}$	$-\frac{1}{2}$	1	0	0	$\frac{1}{2}$	$-\frac{1}{2}$	$-\frac{1}{3}$	$\frac{1}{3}$
$\sqrt{40}Q_i^N$	1	1	2	2	1	0	5	−2	−3	−2	−3

normalized Abelian charge assignment are summarized in Table I. To suppress tree-level flavor-changing transitions and the most dangerous baryon and lepton number violating operators in the E$_6$SSM, an approximate Z_2^H symmetry can be imposed. Under this symmetry all superfields except one pair of H_i^u and H_i^d (i.e. H_u and H_d) and one of the SM-type singlet superfields S_i (i.e. S) are odd. When all Z_2^H symmetry violating couplings are small, this discrete symmetry allows one to suppress flavor-changing processes. If the Lagrangian of the E$_6$SSM is invariant with respect to either a Z_2^L symmetry, under which all superfields except leptons are even, or a Z_2^B discrete symmetry that implies that exotic quark and lepton superfields are odd whereas the others remain even, then the most dangerous baryon and lepton number violating operators get forbidden and proton is sufficiently long-lived [3,4]. The presence of exotic matter predicted by the E$_6$SSM at the TeV scale may lead to spectacular new physics signals at the LHC which were analyzed in [3,4,6]. Recently, the particle spectrum and collider signatures associated with it were studied within the constrained version of the E$_6$SSM (cE$_6$SSM) [7]. The threshold corrections to the running gauge and Yukawa couplings in the E$_6$SSM and cE$_6$SSM were studied in detail in [8]. The renormalization of VEVs in the E$_6$SSM was considered in [9].

In this article, we explore the two-loop renormalization group (RG) flow of the gauge and Yukawa couplings within the E_6 inspired supersymmetric extensions of the SM with extra $U(1)_N$ gauge symmetry in which a single discrete $\tilde{Z}_2^H$ symmetry forbids tree-level flavor-changing transitions and the most dangerous baryon and lepton number violating operators [10]. Two different scenarios A and B, that involve extra matter beyond the MSSM contained in three and four $5+\bar{5}$ representations of $SU(5)$, respectively, together with three SM singlets with $U(1)_N$ charges, are considered. These scenarios lead to different phenomenological implications associated with the exotic quarks D_i and $\bar{D}_i$. In the case of scenario A, we demonstrate that the solutions of the RG equations for the $SU(2)_W$ and $U(1)_Y$ gauge couplings tend to converge towards the quasifixed points which are rather close to the experimentally measured low-energy values of these couplings, while the convergence of the corresponding solutions for the strong gauge coupling to the quasifixed point is rather weak. In scenario B, the values of the strong gauge coupling $g_3(Q)$ near the EW scale tend to be substantially smaller than the experimentally measured central value of this coupling. This implies that the values of $\alpha_3(M_Z)$, which are within one standard deviation of its measured central value, result in the appearance of the Landau pole below the grand unification theory (GUT) scale in this scenario. Thus the gauge coupling unification gets basically spoiled by large two-loop corrections in this case.

We also argue that the solutions for the Yukawa couplings approach the quasifixed points with increasing their values at the GUT scale M_X. In contrast with the MSSM, the quasifixed point scenarios in the SUSY models being considered here, that correspond to $\tan\beta \sim 1$, have not been ruled out. In other words, these scenarios can lead to the solutions with the SM-like Higgs mass around ∼125 GeV. We calculate the two-loop upper bounds on the lightest Higgs boson mass in the vicinity of the quasifixed points in these models and compare the obtained results with the corresponding ones in the next-to-minimal supersymmetric Standard Model (NMSSM). Although we focus primarily on the part of the parameter space where the lightest Higgs boson mass attains its maximal value in the SUSY models mentioned above (see, for example, [11,12]), our analysis indicates that the values of the Yukawa couplings near the quasifixed points are such that the SM-like Higgs state has a mass which is lower than 130 GeV for TeV top squark masses.

The layout of the remainder of the paper is as follows. In the next section, we briefly review the E_6 inspired SUSY models with exact custodial $\tilde{Z}_2^H$ symmetry. In Sec. 3, the RG flow of the gauge and Yukawa couplings is studied, and the two-loop upper bounds on the lightest Higgs boson mass in the vicinity of the quasifixed points are calculated. Section 4 concludes the paper.

II. E_6 inspired SUSY models with exact $\tilde{Z}_2^H$ symmetry

In this section, we briefly review the E_6 inspired SUSY models with exact custodial $\tilde{Z}_2^H$ symmetry [10]. These models imply that near some high-energy scale (M_X) E_6 or its subgroup is broken down to $SU(3)_C \times SU(2)_W \times U(1)_Y \times U(1)_\psi \times U(1)_\chi$. Below GUT scale M_X, the particle content of the considered models involves three copies of 27_i-plets and a set of M_l and $\bar{M}_l$ supermultiplets from the incomplete $27'_l$ and $\overline{27'}_l$ representations of E_6.[1] All matter superfields, that fill in complete 27_i-plets, are odd under $\tilde{Z}_2^H$

[1]Because multiplets M_l and $\bar{M}_l$ have opposite $U(1)_Y$, $U(1)_\psi$, and $U(1)_\chi$ charges, their contributions to the anomalies get canceled identically.

discrete symmetry, while the supermultiplets $\bar{M}_l$ can be either odd or even. All supermultiplets M_l are even under the $\tilde{Z}_2^H$ symmetry and therefore can be used for the breakdown of gauge symmetry. In order to ensure that the $SU(2)_W \times U(1)_Y \times U(1)_\psi \times U(1)_\chi$ symmetry is broken down to $U(1)_{em}$ associated with the electromagnetism, the set of multiplets M_l should involve H_u, H_d, S, and N_H^c.

These E_6 inspired SUSY models also imply that just below the GUT scale $U(1)_\psi \times U(1)_\chi$ gauge symmetry is broken by the VEVs of N_H^c and $\bar{N}_H^c$ down to $U(1)_N \times Z_2^M$, where $Z_2^M = (-1)^{3(B-L)}$ is a matter parity. This can be easily arranged, because matter parity is a discrete subgroup of $U(1)_\psi$ and $U(1)_\chi$. Such a breakdown of $U(1)_\psi$ and $U(1)_\chi$ gauge symmetries guarantees that the exotic states which originate from 27_i representations of E_6 as well as ordinary quark and lepton states survive to low energies. The large VEVs of N_H^c and $\bar{N}_H^c$ can induce the large Majorana masses for right-handed neutrinos allowing them to be used for the seesaw mechanism. Since N_H^c and $\bar{N}_H^c$ acquire VEVs, both supermultiplets must be even under the $\tilde{Z}_2^H$ symmetry.

Here we restrict our consideration to the simplest scenarios in which $\bar{H}_u$, $\bar{H}_d$, and $\bar{S}$ are odd under the $\tilde{Z}_2^H$ symmetry and $\bar{S}$ from the $\overline{27'}_l$ gets combined with the superposition of the corresponding components from 27_i resulting in the vectorlike states with masses of the order of M_X. At low energies (i.e. TeV scale) the superfields H_u, H_d, and S play the role of Higgs fields. The VEVs of these superfields ($\langle H_d \rangle = v_1/\sqrt{2}$, $\langle H_u \rangle = v_2/\sqrt{2}$, and $\langle S \rangle = s/\sqrt{2}$) break the $SU(2)_W \times U(1)_Y \times U(1)_N$ gauge symmetry down to $U(1)_{em}$. The $\tilde{Z}_2^H$ symmetry allows the Yukawa interactions in the superpotential that originate from $27'_l \times 27'_m \times 27'_n$ and $27'_l \times 27_i \times 27_k$. Since the set of multiplets M_l contains only one pair of doublets H_d and H_u, the $\tilde{Z}_2^H$ symmetry defined above forbids flavor-changing processes at the tree level. Nonetheless, if the set of $\tilde{Z}_2^H$ even supermultiplets M_l involve only H_u, H_d, S, and N_H^c, then the lightest exotic quarks are extremely long-lived particles, because $\tilde{Z}_2^H$ symmetry forbids all Yukawa interactions in the superpotential that can allow the lightest exotic quarks to decay.[2]

To ensure that the lightest exotic quarks decay within a reasonable time, the set of $\tilde{Z}_2^H$ even supermultiplets M_l can be supplemented by either L_4 (scenario A) or d_4^c (scenario B). In both cases, it is assumed that at low energies extra matter beyond the MSSM fills in complete $SU(5)$ representations to preserve gauge coupling unification which remains almost exact in the one-loop approximation if this condition is fulfilled. In scenario A, this requires that $\bar{H}_u$ and $\bar{H}_d$ from the $\overline{27'}_l$ get combined with the superposition of the corresponding components from 27_i forming vectorlike states which gain masses $\sim M_X$. The supermultiplets L_4 and $\bar{L}_4$ are also expected to form vectorlike states. However, these states are required to be light enough to ensure that the lightest exotic quarks decay sufficiently fast.[3] In this case, the baryon and lepton number conservation requires exotic quarks to be leptoquarks. The low-energy matter content in scenario A involves

$$3[(Q_i, u_i^c, d_i^c, L_i, e_i^c)] + 3(D_i, \bar{D}_i) + 2(S_\alpha) + 2(H_\alpha^u) + 2(H_\alpha^d) + L_4 + \bar{L}_4 + S + H_u + H_d, \tag{2}$$

where $\alpha = 1, 2$ and $i = 1, 2, 3$. Neglecting all suppressed nonrenormalizable interactions, one gets an explicit expression for the superpotential in this case:

$$W_A = \lambda S(H_u H_d) + \lambda_{\alpha\beta} S(H_\alpha^d H_\beta^u) + \kappa_{ij} S(D_i \bar{D}_j) + \tilde{f}_{\alpha\beta} S_\alpha (H_\beta^d H_u) + f_{\alpha\beta} S_\alpha (H_d H_\beta^u) + g_{ij}^D (Q_i L_4) \bar{D}_j + h_{i\alpha}^E e_i^c (H_\alpha^d L_4) + \mu_L L_4 \bar{L}_4 + W_{\rm MSSM}(\mu = 0). \tag{3}$$

In scenario B, extra matter beyond the MSSM fills in complete $SU(5)$ representations if $\bar{H}_u$, $\bar{H}_d$, d_4^c, and $\overline{d^c}_4$ survive to the TeV scale. In the simplest case, $\bar{H}_u$ and $\bar{H}_d$ are odd under the $\tilde{Z}_2^H$ symmetry so that they do not acquire VEVs. In contrast, d_4^c and $\overline{d^c}_4$ are expected to be $\tilde{Z}_2^H$ even superfields, since these supermultiplets should give rise to the decays of the lightest exotic color states. In this case, the exotic quarks are allowed to have nonzero Yukawa couplings with a pair of quarks. They can also interact with d_4^c and right-handed neutrinos. If Majorana right-handed neutrinos are very heavy ($\sim M_X$), then the interactions of exotic quarks with leptons are extremely suppressed so that $\bar{D}_i$ and D_i manifest themselves in the Yukawa interactions as superfields with baryon number ($\pm\frac{2}{3}$). When the Yukawa couplings of d_4^c are small enough (i.e. less than 10^{-5}–10^{-4}), then the baryon and lepton number violating operators are suppressed and the proton is sufficiently long-lived. In scenario B, the low-energy matter content may be summarized as

$$3[(Q_i, u_i^c, d_i^c, L_i, e_i^c)] + 3(D_i, \bar{D}_i) + 3(H_i^u) + 3(H_i^d) + 2(S_\alpha) + d_4^c + \overline{d^c}_4 + H_u + \bar{H}_u + H_d + \bar{H}_d + S, \tag{4}$$

[2]The models with stable charged exotic particles are ruled out by different terrestrial experiments [13].

[3]The appropriate mass term $\mu_L L_4 \bar{L}_4$ in the superpotential can be induced within supergravity models just after the breakdown of local SUSY if the Kähler potential contains an extra term $(Z_L(L_4 \bar{L}_4) + \text{H.c.})$ [14].

TABLE II. Transformation properties of different components of E_6 multiplets under $\tilde{Z}_2^H$, Z_2^M, and Z_2^E discrete symmetries.

	27_i	27_i	$27'_{H_u}$ $(27'_{H_d})$	$27'_S$	$\overline{27'}_{H_u}$ $(\overline{27'}_{H_d})$	$\overline{27'}_S$	$27'_N$ $(\overline{27'}_N)$	$27'_L$ $(\overline{27'}_L)$	$27'_d$ $(\overline{27'}_d)$
	$Q_i, u_i^c, d_i^c,$ L_i, e_i^c, N_i^c	$\bar{D}_i, D_i,$ H_i^d, H_i^u, S_i	H_u (H_d)	S	$\bar{H}_u$ $(\bar{H}_d)$	$\bar{S}$	N_H^c $(\bar{N}_H^c)$	L_4 $(\bar{L}_4)$	d_4^c $(\bar{d}^c{}_4)$
$\tilde{Z}_2^H$	$-$	$-$	$+$	$+$	$-$	$-$	$+$	$+$	$+$
Z_2^M	$-$	$+$	$+$	$+$	$+$	$+$	$-$	$-$	$-$
Z_2^E	$+$	$-$	$+$	$+$	$-$	$-$	$-$	$-$	$-$

whereas the renormalizable part of the TeV scale superpotential is given by

$$W_B = \lambda S(H_u H_d) + \lambda_{ij} S(H_i^d H_j^u) + \kappa_{ij} S(D_i \bar{D}_j) + \tilde{f}_{\alpha i} S_\alpha (H_i^d H_u) + f_{\alpha i} S_\alpha (H_d H_i^u) + g_{ij}^q \bar{D}_i d_4^c u_j^c + h_{ij}^D d_4^c (H_i^d Q_j) + \mu_d d_4^c \bar{d}^c{}_4 + \mu_i^u H_i^u \bar{H}_u + \mu_i^d H_i^d \bar{H}_d + W_{\rm MSSM}(\mu = 0). \quad (5)$$

The superpotential (5) contains a set of the TeV scale mass parameters, i.e. μ_d, μ_i^u, μ_i^d, that can be induced after the breakdown of local SUSY.

The gauge group and field content of the E_6 inspired SUSY models discussed above can originate from the 5D and 6D orbifold GUT models in which the splitting of GUT multiplets can be naturally achieved [10]. In these orbifold GUT models, all GUT relations between the Yukawa couplings can get entirely spoiled. On the other hand, the approximate unification of the SM gauge couplings should take place in these models. In scenario A, the analysis of the solutions of the two-loop RG equations indicates that the gauge coupling unification can be achieved for any phenomenologically reasonable value of $\alpha_3(M_Z)$ consistent with the central measured low-energy value [10,15]. In scenario B, large two-loop corrections spoil the exact unification of gauge couplings [10]. Nonetheless, the relative discrepancy of $\alpha_i(M_X)$ is about 10% that should not be probably considered as a big problem within the orbifold GUT framework.

The invariance of the low-energy effective Lagrangian of the E_6 inspired SUSY models being considered here under both Z_2^M and $\tilde{Z}_2^H$ symmetries implies that it is also invariant under the transformations of Z_2^E symmetry associated with exotic states because $\tilde{Z}_2^H = Z_2^M \times Z_2^E$. The transformation properties of different components of 27_i, $27'_l$, and $\overline{27'}_l$ supermultiplets under the $\tilde{Z}_2^H$, Z_2^M, and Z_2^E symmetries are summarized in Table II. The Z_2^E symmetry conservation implies that in collider experiments the exotic particles, which are odd under this symmetry, can be created only in pairs and the lightest exotic state must be stable. By using the method proposed in [16], it was argued that the masses of the lightest and second lightest inert neutralino states ($\tilde{H}_1^0$ and $\tilde{H}_2^0$), which are predominantly the fermion components of the two SM singlet superfields S_i from 27_i, do not exceed 60–65 GeV [17]. Since these states are odd under the Z_2^E symmetry, they tend to be the lightest exotic particles in the spectrum [17].

On the other hand, the Z_2^M symmetry conservation ensures that R parity is also conserved. Because $\tilde{H}_1^0$ is also the lightest R-parity odd state, either the lightest R-parity even exotic state or the lightest R-parity odd state with $Z_2^E = +1$ must be absolutely stable. Most commonly, the second stable state is the lightest ordinary neutralino χ_1^0 ($Z_2^E = +1$). Although both stable states are natural dark matter candidates in these E_6 inspired SUSY models, the couplings of $\tilde{H}_1^0$ to the gauge bosons, Higgs states, quarks, and leptons are rather small when $|m_{\tilde{H}_1^0}| \ll M_Z$. As a consequence, the cold dark matter density tends to be much larger than its measured value. In principle, $\tilde{H}_1^0$ could account for all or some of the observed cold dark matter density if it had mass close to half the Z mass [17,18]. However, the usual SM-like Higgs boson decays more than 95% of the time into either $\tilde{H}_1^0$ or $\tilde{H}_2^0$ in these cases [17]. Thus, the corresponding scenarios are basically ruled out nowadays.

The simplest phenomenologically viable scenarios imply that $f_{\alpha\beta} \sim \tilde{f}_{\alpha\beta} \lesssim 10^{-6}$ [10]. So small values of the Yukawa couplings $f_{\alpha\beta}$ and $\tilde{f}_{\alpha\beta}$ result in extremely light inert neutralino states $\tilde{H}_1^0$ and $\tilde{H}_2^0$ which are substantially lighter than 1 eV.[4] In this case, $\tilde{H}_1^0$ and $\tilde{H}_2^0$ form hot dark matter (dark radiation) in the Universe but give only a very minor contribution to the dark matter density, while the lightest ordinary neutralino may account for all or some of the observed dark matter density.

III. THE RG FLOW OF THE GAUGE AND YUKAWA COUPLINGS

In this section, we consider the RG flow of the gauge and Yukawa couplings in the case of scenarios A and B. The superpotential in the E_6 inspired SUSY models discussed in the previous section involves a lot of new Yukawa couplings in comparison to the SM and MSSM. New

[4]The presence of very light neutral fermions in the particle spectrum might have interesting implications for the neutrino physics (see, for example, [19]).

couplings may be relatively large, affecting the running of all parameters. This complicates the analysis of the RG flow drastically, making it model dependent. Therefore, we restrict our consideration here by the simplest scenarios that allow one to get phenomenologically viable solutions. The top-quark mass measurements clearly indicate that the top-quark Yukawa coupling is large and cannot be ignored. Nevertheless, the theoretical analysis performed in [20,21] revealed that a broad class of solutions of the MSSM RG equations concentrated near the quasifixed point corresponds to $\tan\beta = 1.3$–1.8. These comparatively small values of $\tan\beta$ lead to the lightest Higgs mass which does not exceed 94 ± 5 GeV [20] nowadays, so a light SM-like Higgs boson is ruled out. Thus, in order to get phenomenologically viable solutions within the E_6 inspired SUSY models studied here, we allow the Yukawa coupling λ to be as large as the top-quark Yukawa coupling [i.e. $\lambda(M_X) \sim h_t(M_X)$]. This should permit us to find self-consistent solutions with the larger mass of the SM-like Higgs state as compared with the MSSM. Moreover, large values of λ can affect the evolution of the soft scalar mass m_S^2 of the singlet field S rather strongly, resulting in negative values of m_S^2 at low energies that trigger the breakdown of $U(1)_N$ symmetry. To simplify our analysis, we further assumed that all other Yukawa couplings are sufficiently small so that they can be neglected in the leading approximation. Then the approximate superpotential studied is given by

$$W \approx \lambda S(H_d H_u) + h_t(H_u Q_3) u_3^c. \tag{6}$$

A. The running of the gauge couplings

First of all, we discuss the evolution of the SM gauge couplings $g_i(Q)$. Their values at the EW scale are fixed by the measurements at the Large Electron-Positron collider (LEP) and other experimental data [22]. Assuming that the gauge coupling unification is preserved, the solutions of the one-loop RG equations for the SM gauge couplings may be presented in the following form:

$$\frac{1}{g_i^2(Q)} = \frac{1}{g_0^2} + \frac{\beta_i}{(4\pi)^2} \ln\frac{M_X^2}{Q^2}, \tag{7}$$

where index i runs from 1 to 3 and β_i are one-loop β functions: $\beta_1 = \frac{33}{5} + n_f$, $\beta_2 = 1 + n_f$, $\beta_3 = -3 + n_f$. Here n_f is a number of pairs of $5 + \bar{5}$ supermultiplets that survive to the TeV scale in addition to the MSSM particle contents. In scenarios A and B, the corresponding numbers are $n_f = 3$ and $n_f = 4$, respectively. Although the high-energy scale M_X where the unification of the SM gauge couplings takes place is almost insensitive to n_f, the overall gauge coupling g_0 depends on the number of exotic supermultiplets n_f rather strongly. It rises when n_f grows. Indeed, in the one-loop approximation we have

$$\frac{1}{g_0^2} = \frac{1}{\beta_1 - \beta_2}\left(\frac{\beta_1}{g_2^2(M_Z^2)} - \frac{\beta_2}{g_1^2(M_Z^2)}\right). \tag{8}$$

For $n_f = 3$ the value of the overall gauge coupling $g_0 \simeq 1.2$, while for $n_f = 4$ Eq. (8) gives $g_0 \simeq 2.0$. If $n_f > 4$, the right-hand side of Eq. (8) becomes negative that restricts a possible number of extra $5 + \bar{5}$ pairs which can survive to the TeV scale by four.

In the case of the $SU(2)_W$ and $U(1)_Y$ gauge couplings, the large values of $g_0^2 \gg 1$ imply that the first term in the right-hand side of Eq. (7) is substantially smaller than the second term and the corresponding solutions of the RG equations are focused near the infrared stable fixed point at low energies, i.e.

$$\frac{g_1^2}{g_2^2} \simeq \frac{\beta_2}{\beta_1}. \tag{9}$$

This fixed point corresponds to $\frac{dg_1/g_2}{dt} \to 0$, where $t = \ln(M_X/Q)$, Q is a renormalization scale. In general, the solutions of the RG equations always approach the infrared stable fixed point when $t \to \infty$. In our analysis, the interval of variations of t remains always finite, i.e. $0 \le t \le \ln\frac{M_X^2}{M_Z^2}$. As a consequence, the solutions for $g_i(Q)$ are concentrated near the quasifixed points which set upper limits on the allowed range of the low-energy values of these couplings caused by the applicability of the perturbation theory up to the scale M_X, i.e. $g_0 \lesssim \sqrt{4\pi}$.

In the case of scenarios A and B, the values of the $SU(2)_W$ and $U(1)_Y$ gauge couplings calculated in the limit $g_0^2 \gg 1$ are relatively close to the measured values of these couplings, i.e. $g_1(M_Z) \simeq 0.461$ and $g_2(M_Z) \simeq 0.652$. The ratio of the measured values of the $SU(2)_W$ and $U(1)_Y$ gauge couplings $g_1^2(M_Z)/g_2^2(M_Z) \simeq 0.5$, whereas Eq. (9) gives $\frac{g_1^2}{g_2^2} \simeq 0.47$ in scenario B and $\frac{g_1^2}{g_2^2} \simeq 0.42$ in scenario A.[5]

If $\beta_3 > 0$, like in scenario B, the solutions of the RG equations for the $SU(2)_W$ and $SU(3)_C$ gauge couplings also approach the fixed point

$$\frac{g_2^2}{g_3^2} \simeq \frac{\beta_3}{\beta_2} \tag{10}$$

in the limit $g_0^2 \to \infty$. However, since even in scenario B the value of the one-loop beta function associated with the strong interactions is rather small, i.e. $\beta_3 = 1$, the convergence of the solutions for $g_3(Q)$ to the corresponding quasifixed point is rather weak. Therefore, the solutions of the RG equations for $g_2(Q)/g_3(Q)$ are also attracted to the

[5]In the MSSM the infrared fixed point (9) is very far from the corresponding ratio of the physical quantities of the $SU(2)_W$ and $U(1)_Y$ gauge couplings. Indeed, for $n_f = 0$, Eq. (9) gives $\frac{g_1^2}{g_2^2} \simeq 0.15$.

TABLE III. The values of the gauge couplings at the EW scale. These couplings are calculated for $g_1(M_X) = g_1'(M_X) = g_2(M_X) = g_3(M_X) = h_t(M_X) = \lambda(M_X) = g_0$, $g_{11}(M_X) = 0$, and different values of g_0 in the two-loop approximation. The low-energy values of the corresponding couplings calculated in the one-loop approximation are given in the brackets.

	g_0	g_3	g_2	g_1	g_1'	g_{11}	$\frac{g_1^2}{g_2^2}$	$\frac{g_1'}{g_1}$
	1.2	1.074	0.628	0.454	0.458	0.0196	0.523	1.0090
	1.5	1.213	0.655	0.465	0.469	0.0210	0.503	1.0090
Scenario A		(1.5)	(0.684)	(0.471)	(0.476)	(0.0219)	(0.474)	(1.0106)
	2.0	1.330	0.676	0.473	0.477	0.0221	0.489	1.0084
	3.0	1.395	0.689	0.478	0.481	0.0228	0.481	1.0074
		(3.0)	(0.744)	(0.489)	(0.495)	(0.0246)	(0.432)	(1.0116)
	1.2	0.881	0.582	0.436	0.431	−0.0254	0.560	0.989
	1.6	0.975	0.609	0.447	0.442	−0.0275	0.539	0.988
Scenario B		(1.108)	(0.632)	(0.453)	(0.448)	(−0.0286)	(0.514)	(0.989)
	2.0	1.020	0.622	0.453	0.447	−0.0285	0.530	0.987
	3.0	1.057	0.633	0.458	0.451	−0.0294	0.523	0.986
		(1.368)	(0.670)	(0.466)	(0.461)	(−0.0312)	(0.484)	(0.989)

fixed point (10) very weakly. In the case of scenario A, β_3 vanishes in the one-loop approximation, so that near the fixed point (10) $\frac{g_2^2}{g_3^2} \to 0$. It means that the ratios $g_{1,2}^2/g_3^2$ become extremely small when $t \to \infty$. At any low-energy scale Q, the value of the strong gauge coupling in scenarios A and B is substantially larger than $g_1(Q)$ and $g_2(Q)$, so that the ratios $g_{1,2}^2/g_3^2$ are quite small but not negligible.

The inclusion of the two-loop corrections shifts the position of the quasifixed points where the solutions of the RG equations are focused. The values of the gauge couplings at the EW scale calculated for different values of g_0 in the two-loop approximation are given in Table III. The two-loop RG flow of gauge couplings is shown in Fig. 1. The corresponding two-loop beta functions can be found in [10]. The results presented in Table 2 demonstrate that the inclusion of the two-loop corrections leads to the growth of the ratio $\frac{g_1^2}{g_2^2}$ near the quasifixed points. Indeed, for $g_0 = 3$ in scenario A $\frac{g_1^2}{g_2^2}$ increases from 0.43 to 0.48, whereas in scenario B $\frac{g_1^2}{g_2^2}$ grows from 0.48 to 0.52.

In the case of scenario A, the typical pattern of the RG flow of the gauge couplings from $Q = M_X$ to the EW scale for different values of g_0 is presented in Fig. 1. The same plots can be obtained in scenario B as well. Since plots in the case of scenarios A and B look very similar, we include only ones that correspond to scenario A. From Fig. 1(a), it follows that the solutions of the RG equations for $g_1(Q)$ and $g_2(Q)$ are sufficiently strongly attracted to the quasifixed points. In scenarios A and B, the numerical values of these gauge couplings associated with the quasifixed points (see Table III) are reasonably close to the measured values of these couplings. On the other hand, as one can see from Fig. 1(b), the convergence of the solutions of the RG equations for $g_3(Q)$ to the quasifixed point is rather weak. Moreover, our numerical analysis reveals that in the case of scenario B the values of $g_3(Q)$ at the EW scale tend to be substantially smaller than the experimentally measured central value of this coupling.[6] In scenario A, the value of $g_3(Q)$, where the solutions of the RG equations are focused at low energies, is considerably larger than the one that corresponds to $\alpha_3(M_Z) \simeq 0.118$. At the same time, the results presented in Table III indicate that for $g_0 = 1.5$ all SM gauge couplings at the EW scale including the strong gauge coupling are rather close to their measured central values in the case of scenario A.

The RG flow of the gauge couplings in scenarios A and B is affected by the kinetic term mixing which is consistent with all symmetries. Indeed, in the most general case, the gauge kinetic part of the Lagrangian can be written as

$$\mathcal{L}_{\rm kin} = -\frac{1}{4}(F_{\mu\nu}^Y)^2 - \frac{1}{4}(F_{\mu\nu}^N)^2 - \frac{\sin\chi}{2} F_{\mu\nu}^Y F_{\mu\nu}^N - \cdots, \quad (11)$$

where $F_{\mu\nu}^Y$ and $F_{\mu\nu}^N$ are field strengths for the $U(1)_Y$ and $U(1)_N$ gauge interactions, while B_μ^Y and B_μ^N are the corresponding gauge fields, respectively. In Eq. (11), the terms associated with the $SU(3)_C$ and $SU(2)_W$ gauge interactions are omitted. If $U(1)_Y$ and $U(1)_N$ symmetries arise from the breaking of the simple gauge group E_6, the parameter $\sin\chi$ which parametrizes the gauge kinetic term mixing is expected to vanish near the GUT scale. Nevertheless, it gets induced due to loop effects, since

$$\mathrm{Tr}(Q^Y Q^N) = \sum_{i=\text{chiral fields}} (Q_i^Y Q_i^N) \neq 0. \quad (12)$$

[6] In scenario B, the considerably larger values of the strong gauge coupling at the EW scale can be obtained if we take into account the low-energy threshold effects associated with the presence of exotic states and superpartners of ordinary particles. Nevertheless, even in this case the exact unification of gauge couplings can be achieved only for $\alpha_3(M_Z) \lesssim 0.112$. For $\alpha_3(M_Z) \simeq 0.118$ the relative discrepancy of $\alpha_i(M_X)$ is about 10%.

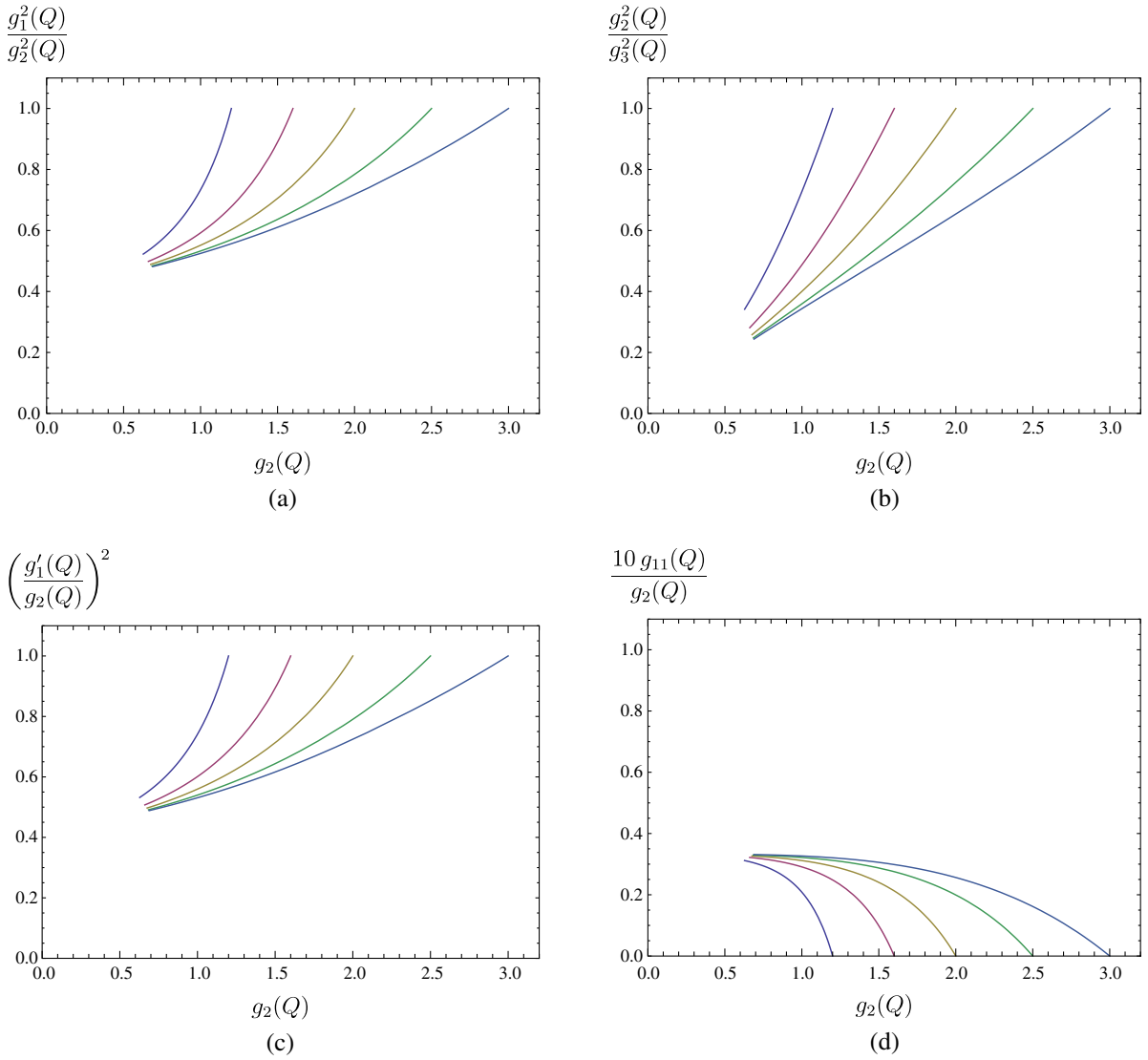

FIG. 1 (color online). Two-loop RG flow of gauge couplings in the case of scenario A for $g_1(M_X) = g_1'(M_X) = g_2(M_X) = g_3(M_X) = h_t(M_X) = \lambda(M_X) = g_0$, $g_{11}(M_X) = 0$, and different values of g_0: (a) evolution of $\frac{g_1^2(Q)}{g_2^2(Q)}$ versus $g_2(Q)$ from $Q = M_X$ to the EW scale; (b) running of $\frac{g_2^2(Q)}{g_3^2(Q)}$ versus $g_2(Q)$ from $Q = M_X$ to the EW scale; (c) RG flow of $\frac{g_1'^2(Q)}{g_2^2(Q)}$ versus $g_2(Q)$ from $Q = M_X$ to the EW scale; (d) running of $\frac{10g_{11}(Q)}{g_2(Q)}$ versus $g_2(Q)$ from $Q = M_X$ to the EW scale.

Here the trace is restricted to the states lighter than the energy scale being considered. The complete E_6 multiplets do not contribute to the trace (12). Its nonzero value is caused by the presence of the components of the incomplete $27_l'$ and $27'_l$ multiplets of the original E_6 symmetry which survive to low energy.

The mixing in the gauge kinetic part of the Lagrangian (11) can be eliminated by a nonunitary transformation of two $U(1)$ gauge fields [23]:

$$B_\mu^Y = B_{1\mu} - B_{2\mu}\tan\chi, \qquad B_\mu^N = B_{2\mu}/\cos\chi. \tag{13}$$

In the new basis of the gauge fields $(B_{1\mu}, B_{2\mu})$, the gauge kinetic part of the Lagrangian is diagonal, whereas the covariant derivative can be written in a compact form:

$$D_\mu = \partial_\mu - iQ^T G B_\mu \ldots, \tag{14}$$

where $Q^T = (Q_i^Y, Q_i^N)$, $B_\mu^T = (B_{1\mu}, B_{2\mu})$, and G is a 2×2 matrix of gauge couplings:

$$G = \begin{pmatrix} g_1 & g_{11} \\ 0 & g_1' \end{pmatrix}, \qquad g_1 = g_Y, \qquad g_1' = g_N/\cos\chi, \qquad g_{11} = -g_Y\tan\chi. \tag{15}$$

In the expression for the covariant derivative (14), the $SU(3)_C$ and $SU(2)_W$ gauge fields are omitted. In Eq. (15), g_Y and g_N are original $U(1)_Y$ and $U(1)_N$ gauge couplings, respectively, which are supposed to be equal at the scale M_X. In the considered approximation the gauge kinetic mixing changes effectively the $U(1)_N$ charges of the fields to $\tilde{Q}_i^N = Q_i^N + Q_i^Y\delta$, where $\delta = g_{11}/g_1'$, while the $U(1)_Y$ charges remain the same.

Using the matrix notation for the structure of $U(1)$ interactions, one can write down the RG equations for the Abelian couplings in a compact form [24]:

$$\frac{dG}{dt} = -G \times B,$$
$$B = \frac{1}{(4\pi)^2}\begin{pmatrix} \beta_1 g_1^2 & 2g_1 g_1' \beta_{11} + 2g_1 g_{11}\beta_1 \\ 0 & g_1'^2\beta_1' + 2g_1' g_{11}\beta_{11} + g_{11}^2\beta_1 \end{pmatrix}. \quad (16)$$

From Eqs. (16), one can see that, whereas the solution of the one-loop RG equation for $g_1(Q)$ is still described by Eq. (7), the running of couplings $g_1'(Q)$ and $g_{11}(Q)$ obeys a quite complicated system of differential equations. In scenario A, $\beta_1' = 47/5$ and $\beta_{11} = -\sqrt{6}/5$ in the one-loop approximation. In the case of scenario B, the one-loop β_1' and β_{11} are 10.9 and $\beta_{11} = 3\sqrt{6}/10$, respectively.

In the E_6 inspired SUSY models with an extra $U(1)_N$ factor, the RG equations (16) have infrared stable fixed points:

$$\frac{g_{11}}{g_1'} = -\frac{\beta_{11}}{\beta_1}, \qquad \frac{g_1^2}{g_1'^2} = \frac{\beta_1'}{\beta_1} - \left(\frac{\beta_{11}}{\beta_1}\right)^2. \quad (17)$$

The solutions of the differential equations (16) approach the fixed points (17) when the overall gauge coupling g_0 and t increase. Since in both scenarios $\beta_1 \simeq \beta_1' \gg \beta_{11}$, the values of the diagonal $U(1)_Y$ and $U(1)_N$ gauge couplings are approximately equal at low energies, whereas the of–diagonal gauge coupling $g_{11}(Q)$ being set to zero at the GUT scale remains rather small at any scale below M_X. Equation (17) indicates that in the case of scenario A g_1 tends to be slightly less than g_1' near the fixed point while in scenario B $g_1 \gtrsim g_1'$.

The two-loop RG flows of $g_1'^2/g_2^2$ and g_{11}/g_2 are shown in Figs. 1(c) and 1(d), respectively, where we set $g_1'(M_X) = g_0$ and $g_{11}(M_X) = 0$. Because $g_{11}(Q) \ll g_i(Q)$ and β_{11} is relatively small as compared with the diagonal beta functions, we neglect two-loop corrections to β_{11}. Again, we include only plots associated with scenario A, because the corresponding plots look rather similar in both scenarios. One can see that Figs. 1(a) and 1(c) are almost identical. This is because $g_1(Q) \simeq g_1'(Q)$. The results presented in Fig. 1 and Table III demonstrate that the inclusion of the two-loop corrections does not change much the position of the fixed points (17). In principle, the two-loop corrections to $\beta_3, \beta_2, \beta_1$, and β_1' as well as the two-loop RG flow of all gauge couplings depend on $h_t(Q)$ and $\lambda(Q)$. However, this dependence is rather weak and can be ignored in the first approximation [15]. Nevertheless, the results presented in Table III and Fig. 1 are obtained for $h_t(M_X) = \lambda(M_X) = g_0$. The evolution of the Yukawa couplings will be considered in the next subsection.

B. The running of the Yukawa couplings and the Higgs mass

Since the RG flow of gauge couplings in the E_6 inspired SUSY models with an extra $U(1)_N$ factor implies that the corresponding quasifixed points of RG equations are reasonably close to the measured values of $g_i(M_Z)$, it is worthwhile to examine the quasifixed point solutions for the Yukawa couplings as well. The Yukawa couplings appearing in the superpotential (6) obey the following two-loop RG equations:

$$\frac{d\lambda}{dt} = \frac{\lambda}{(4\pi)^2}\left[-4\lambda^2 - 3h_t^2 + 3g_2^2 + \frac{3}{5}g_1^2 + \frac{19}{10}g_1'^2 - \frac{1}{(4\pi)^2}\left\{-10\lambda^4 - 9\lambda^2 h_t^2 - 9h_t^4 + \lambda^2\left(6g_2^2 + \frac{6}{5}g_1^2 + \frac{13}{10}g_1'^2\right)\right.\right.$$
$$\left.\left. + h_t^2\left(16g_3^2 + \frac{4}{5}g_1^2 - \frac{3}{10}g_1'^2\right) + b_\lambda g_2^4 + c_\lambda g_1^4 + d_\lambda g_1'^4 + \frac{9}{5}g_2^2 g_1^2 + \frac{39}{20}g_2^2 g_1'^2 + \frac{39}{100}g_1^2 g_1'^2\right\}\right],$$
$$\frac{dh_t}{dt} = \frac{h_t}{(4\pi)^2}\left[-\lambda^2 - 6h_t^2 + \frac{16}{3}g_3^2 + 3g_2^2 + \frac{13}{15}g_1^2 + \frac{3}{10}g_1'^2 - \frac{1}{(4\pi)^2}\left\{-3\lambda^4 - 3\lambda^2 h_t^2 - 22h_t^4 + \frac{3}{2}\lambda^2 g_1'^2 + h_t^2(16g_3^2 + 6g_2^2 + \frac{6}{5}g_1^2\right.\right.$$
$$\left.\left. + \frac{3}{10}g_1'^2) + a_{h_t} g_3^4 + b_{h_t} g_2^4 + c_{h_t} g_1^4 + d_{h_t} g_1'^4 + 8g_3^2 g_2^2 + \frac{136}{45}g_3^2 g_1^2 + \frac{8}{15}g_3^2 g_1'^2 + g_2^2 g_1^2 + \frac{3}{4}g_2^2 g_1'^2 + \frac{53}{300}g_1^2 g_1'^2\right], \quad (18)$$

where in the case of scenario A

$$a_\lambda = 0, \quad b_\lambda = \frac{33}{2}, \quad c_\lambda = \frac{297}{50}, \quad d_\lambda = \frac{3933}{200},$$
$$a_{h_t} = \frac{128}{9}, \quad b_{h_t} = \frac{33}{2}, \quad c_{h_t} = \frac{3913}{450}, \quad d_{h_t} = \frac{573}{200}, \quad (19)$$

while in scenario B we have

$$a_\lambda = 0, \quad b_\lambda = \frac{39}{2}, \quad c_\lambda = \frac{327}{50}, \quad d_\lambda = \frac{4503}{200},$$
$$a_{h_t} = \frac{176}{9}, \quad b_{h_t} = \frac{39}{2}, \quad c_{h_t} = \frac{4303}{450}, \quad d_{h_t} = \frac{663}{200}. \quad (20)$$

In the right-hand side of Eq. (18), we neglect all Yukawa couplings except λ and h_t.

From Eq. (18), it follows that the evolution of $\lambda(Q)$ and $h_t(Q)$ depends on the values of the gauge couplings. In the case of scenario A, we set $g_0 = 1.5$. As was pointed out in the previous subsection, this value of the overall gauge coupling leads to $g_i(M_Z)$ which are very close to their measured central values. In scenario B, we fix $g_0 = 3$, because it results in the most phenomenologically acceptable values of gauge couplings at low energies.

For the purposes of our RG studies, it is convenient to introduce

$$\rho_t = \frac{h_t^2}{g_3^2}, \qquad \rho_\lambda = \frac{\lambda^2}{g_3^2}. \tag{21}$$

The allowed range of the parameter space in the (ρ_t, ρ_λ) plane is limited at the EW scale by the quasifixed (or Hill-type effective) line. Outside this range, the solutions for $h_t(Q)$ and $\lambda(Q)$ develop a Landau pole below the scale M_X, so that the perturbation theory becomes inapplicable. The solutions of the RG equations (18) are gathered near this line, when the Yukawa couplings at the GUT scale M_X increase. However, the allocation of the solutions for ρ_t and ρ_λ at the EW scale along the Hill line is not uniform. The main reason for this is that at large values of the Yukawa couplings at the scale M_X the corresponding solutions are attracted not only to the Hill line but also to the invariant (or infrared fixed) line. When t goes to zero, this line approaches its asymptotic limit where $\rho_t, \rho_\lambda \gg 1$ and $\rho_\lambda \to \rho_t$, which is a fixed point of the RG equations for the Yukawa couplings in the gaugeless limit ($g_1 = g_2 = g_3 = g_1' = 0$). The invariant line connects this fixed point with the infrared stable fixed point. In scenario A this fixed point is given by

$$\rho_\lambda = 0, \qquad \rho_t \simeq 0.89. \tag{22}$$

whereas in scenario B

$$\rho_\lambda = 0, \qquad \rho_t \simeq 1.17. \tag{23}$$

All solutions of the RG equations for ρ_t and ρ_λ are concentrated near the infrared stable fixed point at very low energies when $t \to \infty$. The infrared fixed line is the RG invariant solution. If the boundary values at $Q = \Lambda$ are such that $h_t(\Lambda)$ and $\lambda(\Lambda)$ belong to the fixed line, the evolution of the Yukawa couplings proceeds further along this line towards the infrared stable fixed point. With increasing of the interval of the RG flow, the solutions of the differential equations (18) are first attracted to the invariant line and then close to or along this line towards the infrared fixed point. Infrared fixed lines and surfaces, as well as their properties, were studied in detail in [25].

As $h_t(M_X)$ and $\lambda(M_X)$ grow, the region at the EW scale in which the solutions of the RG equations for ρ_t and ρ_λ are concentrated shrinks drastically. They are focused near the intersection point of the invariant and quasifixed lines. Hence this point can be considered as the quasifixed point of the RG equations (18) [26]. In the two-loop approximation, the intersection points of the invariant and quasifixed lines have the following coordinates in the (ρ_t, ρ_λ) plane:

$$\begin{aligned} &(\mathrm{A})\rho_t = 1.16, \qquad \rho_\lambda = 0.14; \qquad (\mathrm{B})\rho_t = 1.33, \\ &\rho_\lambda = 0.18. \end{aligned} \tag{24}$$

in the cases of scenarios A and B, respectively. The quasifixed points ([30]) correspond to $h_t(M_X) = \lambda(M_X) \simeq 3$, i.e. $\rho_\lambda(M_X) = \rho_t(M_X)$, which is associated with the fixed point of the RG equations for the Yukawa couplings in the gaugeless limit. Equation (24) indicates that turning the gauge couplings on induces a certain hierarchy between $h_t(Q)$ and $\lambda(Q)$. Indeed, because $g_3(Q)$ is substantially larger than other gauge couplings at low energies, the top-quark Yukawa coupling tends to dominate over $\lambda(Q)$.

The two-loop RG flows of $\rho_t(Q)$ and $\rho_\lambda(Q)$ in the cases of scenarios A and B are shown in Figs. 2(a) and 2(b). The results of our analysis are also summarized in Table IV. In Figs. 2(a) and 2(b), we plot the running $\rho_\lambda(Q)$ versus $\rho_t(Q)$ from $Q = M_X$ to the EW scale for regular distribution of boundary conditions for $\lambda(M_X)$ and $h_t(M_X)$ at the GUT scale. These plots demonstrate that the trajectories, which represent different solutions of the two-loop RG equations, are focused in a narrow region near the quasifixed points at low energies. From Table IV, it follows that the relative variations of $h_t(M_Z)$ near the quasifixed point are rather small, i.e. about 1%, when $1.5 \lesssim h_t(M_X), \lambda(M_X) \lesssim 3$. The interval of variations of $\lambda(M_Z)$ is substantially wider. The relative deviations of $\lambda(M_Z)$ can be as large as 20% when $h_t(M_X)$ and $\lambda(M_X)$ vary from 1.5 to 3. As one can see from Fig. 2(a), in scenario A different trajectories also tend to flow towards the invariant line that corresponds to $\rho_\lambda(M_X) = \rho_t(M_X) = 4$. This is less obvious in the case of scenario B, since $g_0 = 3$ and the Yukawa couplings $h_t(M_X)$ and $\lambda(M_X)$ have to be either of the order of or even smaller than the gauge ones to ensure the validity of the perturbation theory. Thus, the gaugeless approximation is inapplicable.

The convergence of $h_t(Q)$ to the quasifixed points (24) allows one to predict the value of the top-quark Yukawa coupling at the EW scale. Then, using the relation between the running mass and Yukawa coupling of the t quark

$$m_t(M_t) = \frac{h_t(M_t)}{\sqrt{2}} v \sin\beta, \tag{25}$$

one can find the value of $\tan\beta$ that corresponds to the quasifixed points (24). In Eq. (24), $v = \sqrt{v_1^2 + v_2^2} = 246$ GeV, $\tan\beta = v_2/v_1$, while v_2 and v_1 are the VEVs

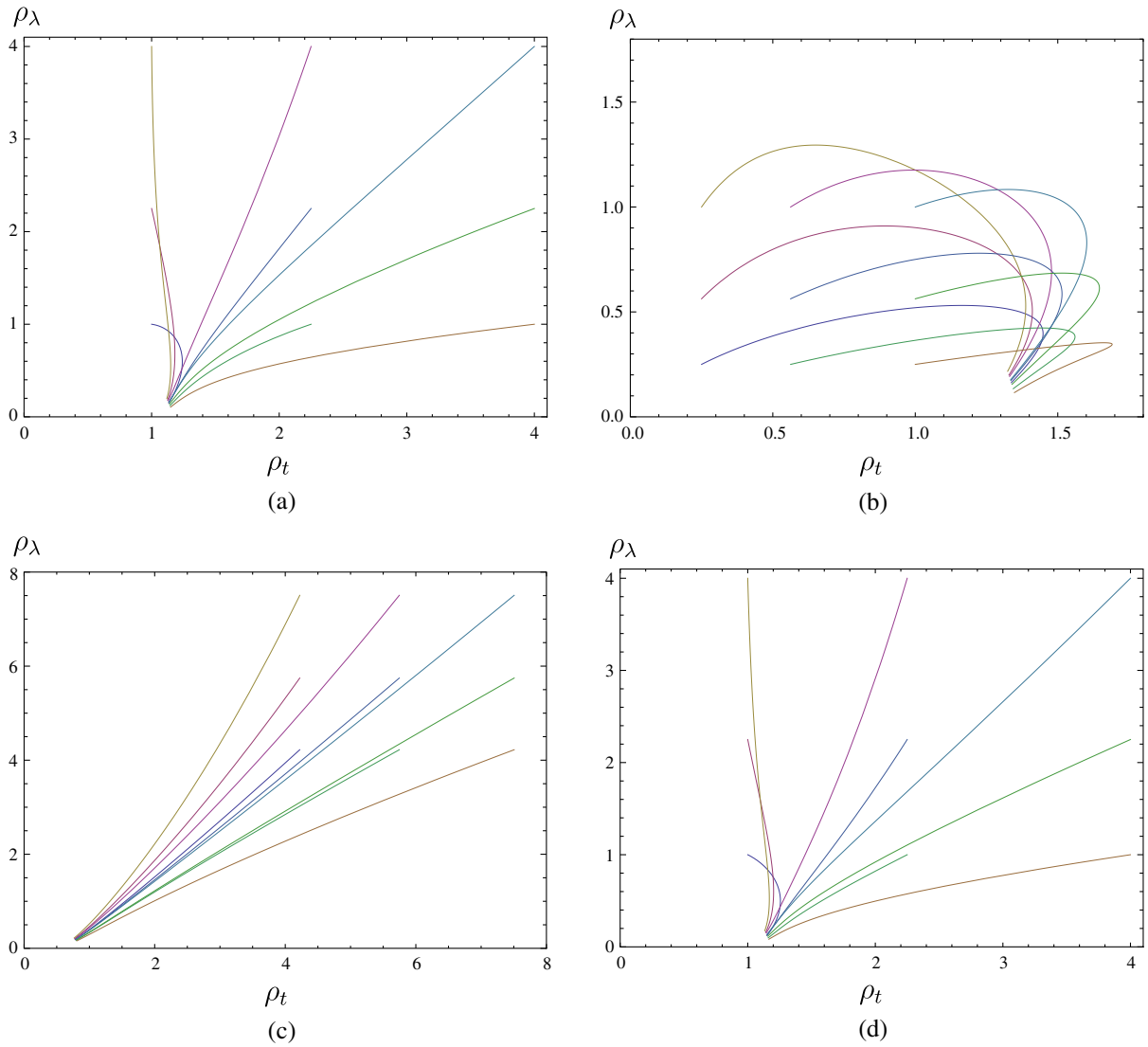

FIG. 2 (color online). (a) Two-loop RG flow of ρ_λ versus ρ_t in scenario A for $g_0 = 1.5$. (b) Two-loop RG flow of the Yukawa couplings in the $\rho_\lambda - \rho_t$ plane in scenario B for $g_0 = 3$. (c) Two-loop RG flow of ρ_λ versus ρ_t within the NMSSM for $g_0 = 0.725$. (d) Two-loop RG flow of the Yukawa couplings in the $\rho_\lambda - \rho_t$ plane within the NMSSM+ for $g_0 = 1.5$. In all cases, the energy scale Q is varied from M_X to M_Z. Different trajectories correspond to different initial conditions for λ and h_t at the scale M_X.

TABLE IV. The values of the Yukawa couplings at the EW scale and the upper bounds on the lightest Higgs mass in scenarios A and B. The values of $h_t(M_Z)$ and $\lambda(M_Z)$ are calculated by using two-loop RG equations for $g_1(M_X) = g_1'(M_X) = g_2(M_X) = g_3(M_X) = g_0$, $g_{11}(M_X) = 0$, and different values of $h_t(M_X)$ and $\lambda(M_X)$. The low-energy values of the Yukawa couplings are used for the calculation of $\tan\beta$, tree-level, and two-loop upper bounds on the mass of the lightest Higgs boson ($m_{h_1}^{(0)}$ and $m_{h_1}^{(2)}$, respectively). We set $m_t(M_t) = 163$ GeV, $M_S = 1200$ GeV, and $X_t = \sqrt{6}M_S$.

	g_0	$h_t(M_X)$	$\lambda(M_X)$	$h_t(M_Z)$	$\lambda(M_Z)$	$\tan\beta$	$m_{h_1}^{(0)}$ (GeV)	$m_{h_1}^{(2)}$ (GeV)
	1.5	3.0	3.0	1.31	0.46	1.02	92.2	120.5
Scenario A	1.5	1.5	3.0	1.30	0.53	1.05	102.4	126.6
	1.5	3.0	1.5	1.32	0.37	1.01	79.0	113.3
	1.5	1.5	1.5	1.31	0.46	1.03	91.7	120.3
	3.0	3.0	3.0	1.22	0.44	1.20	88.7	119.1
Scenario B	3.0	1.5	3.0	1.21	0.49	1.22	95.7	123.2
	3.0	3.0	1.5	1.23	0.36	1.19	76.6	112.3
	3.0	1.5	1.5	1.22	0.43	1.20	86.0	117.5

that Higgs doublets H_u and H_d develop. In our analysis, we set $m_t(M_t) \simeq 163$ GeV, which is rather close to the central value that can be obtained by using the world average mass of the top quark $M_t = 173.07 \pm 0.52 \pm 0.72$ GeV (see [22]) and the relationship between the t-quark pole (M_t) and running [$m_t(Q)$] masses [27]

$$m_t(M_t) = M_t\left[1 - 1.333\frac{\alpha_s(M_t)}{\pi} - 9.125\left(\frac{\alpha_s(M_t)}{\pi}\right)^2\right]. \tag{26}$$

From Table IV, one can see that $\tan\beta = 1.02$–1.05 in scenario A and $\tan\beta = 1.19$–1.22 in scenario B when $h_t(M_X)$ and $\lambda(M_X)$ vary from 1.5 to 3.

The spectrum of the Higgs bosons in the E_6 inspired SUSY models with an extra $U(1)_N$ factor involves a set of the neutral Higgs states. Like in the MSSM, one of the neutral CP-even Higgs states, which manifests itself in the interactions with gauge bosons and fermions as a SM-like Higgs boson, is always light irrespective of the SUSY breaking scale. In the leading approximation, the two-loop upper bound on the mass of the lightest Higgs particle in the E_6 inspired SUSY models with extra $U(1)_N$ symmetry can be written as [3]

$$\begin{aligned} m^2_{h_1} \le & \left[\frac{\lambda^2}{2}v^2\sin^2 2\beta + M_Z^2\cos^2 2\beta + g_1'^2 v^2\left(\tilde{Q}_1\cos^2\beta\right.\right. \\ & \left.\left. + \tilde{Q}_2\sin^2\beta\right)^2\right]\left(1 - \frac{3h_t^2}{8\pi^2}l\right) + \frac{3h_t^4 v^2\sin^4\beta}{8\pi^2} \\ & \times\left\{\frac{1}{2}U_t + l + \frac{1}{16\pi^2}\left(\frac{3}{2}h_t^2 - 8g_3^2\right)(U_t + l)l\right\}, \\ U_t = & \, 2\frac{X_t^2}{M_S^2}\left(1 - \frac{1}{12}\frac{X_t^2}{M_S^2}\right), \qquad l = \ln\left[\frac{M_S^2}{m_t^2}\right], \end{aligned} \tag{27}$$

where $\tilde{Q}_1$ and $\tilde{Q}_2$ are effective $U(1)_N$ charges of H_d and H_u, respectively, X_t is a top squark mixing parameter, M_S is a SUSY breaking scale defined as $m_Q^2 = m_U^2 = M_S^2$, and m_Q^2 and m_U^2 are soft scalar masses of superpartners of the left-handed and right-handed components, respectively, of the t quark. Equation (27) is a simple generalization of the approximate expressions for the upper bounds on the lightest Higgs boson mass obtained in the MSSM [28] and NMSSM [29]. At $\lambda = 0$ and $g_1' = 0$, the right-hand side of Eq. (27) coincides with the theoretical bound on the lightest Higgs mass in the MSSM which does not exceed the Z-boson mass ($M_Z \simeq 91.2$ GeV) at the tree level [30]. Leading one-loop and two-loop corrections to m_{h_1} increase the upper bound on the lightest Higgs boson mass from M_Z to 130 GeV (see [31] and references therein). In the MSSM the approximate expression (27) leads to the value of the lightest Higgs mass which is typically a few GeV lower than the one which is computed by using the SUSPECT [32] and FEYNHIGGS [33] packages.

In our analysis, we focus on the so-called maximal mixing scenario, when $X_t = \sqrt{6}M_S$, that leads to the maximal possible value of m_{h_1}. We also set top squark scalar masses to be equal to $m_Q = m_U = M_S = 1200$ GeV that result in the reasonably light top squarks which are not ruled by the LHC experiments. Then for each set of $\lambda(M_Z)$ and $\tan\beta$ one can calculate the theoretical restriction on m_{h_1}. The analysis performed in [3] shows that in this case the two-loop upper bound on the lightest Higgs mass reaches its maximal value, i.e. 150–155 GeV, for $\tan\beta \simeq 1.5$–2 when the low-energy value of the coupling λ can be as large as 0.7–0.8. The results presented in Table IV indicate that the quasifixed point solutions in scenarios A and B correspond to substantially lower values of $\tan\beta$ and $\lambda(M_Z)$. Therefore the two-loop upper bound on the lightest Higgs mass is also considerably lower than 155 GeV. On the other hand, in order to get solutions which can be consistent with the observation of the SM-like Higgs state with mass around ~125 GeV, the values of the coupling $\lambda(M_Z)$ should be larger than $g_1'(M_Z)$ at least. From Table IV, one can see that it is possible to find such solutions in the vicinity of the quasifixed point in the case of scenario A. In scenario B, the low-energy values of $\lambda(M_Z)$ are typically smaller than the ones in scenario A, and it seems to be rather problematic to find phenomenologically acceptable solutions near the corresponding quasifixed point.

The requirement that $\lambda \gtrsim g_1'$ at the EW scale leads to extremely hierarchical structure of the Higgs spectrum [3]. Indeed, in this case the qualitative pattern of the Higgs spectrum is rather similar to the one that arises in the Peccei-Quinn symmetric NMSSM in which the heaviest CP-even, CP-odd, and charged states are almost degenerate and much heavier than the lightest and second lightest CP-even Higgs bosons [34,35]. Because the mass of the second lightest CP-even Higgs state is set by the Z' boson mass ($M_{Z'}$) [3], which should be heavier than 2 TeV, the heaviest Higgs boson masses lie beyond the multi-TeV range, and the mass matrix of the CP-even Higgs sector can be diagonalized by using the perturbation theory [35,36]. Thus the phenomenologically viable quasifixed point solutions in the E_6 inspired SUSY models with extra $U(1)_N$ gauge symmetry imply that all Higgs states except the lightest one are extremely heavy and cannot be discovered at the LHC. In this limit the lightest CP-even Higgs boson is the analogue of the SM Higgs field. Extremely hierarchical structure of the Higgs spectrum also implies that all phenomenologically viable quasifixed point scenarios are quite fine-tuned.

It is useful to compare the results of our analysis of the quasifixed point scenarios in the E_6 inspired SUSY models with the corresponding results in more simple SUSY extensions of the SM like the NMSSM [37] and its modifications [38]. In the NMSSM, the spectrum of the MSSM is extended by one singlet superfield (for reviews

TABLE V. The values of the Yukawa couplings at the EW scale and the upper bounds on the lightest Higgs mass in the NMSSM and NMSSM+. The values of $h_t(M_Z)$ and $\lambda(M_Z)$ are calculated by using two-loop RG equations for $g_1(M_X) = g_2(M_X) = g_3(M_X) = g_0$ and different values of $h_t(M_X)$ and $\lambda(M_X)$. The low-energy values of the Yukawa couplings are used for the calculation of $\tan\beta$, tree-level, and two-loop upper bounds on the mass of the lightest Higgs boson ($m_{h_1}^{(0)}$ and $m_{h_1}^{(2)}$, respectively). We set $m_t(M_t) = 163$ GeV, $M_S = 1200$ GeV, and $X_t = \sqrt{6}M_S$.

	g_0	$h_t(M_X)$	$\lambda(M_X)$	$h_t(M_Z)$	$\lambda(M_Z)$	$\tan\beta$	$m_{h_1}^{(0)}$ (GeV)	$m_{h_1}^{(2)}$ (GeV)
	0.725	3.0	3.0	1.10	0.54	1.60	93.4	122.5
NMSSM	0.725	1.5	3.0	1.06	0.62	1.90	102.8	128.9
	0.725	3.0	1.5	1.12	0.43	1.52	77.8	113.2
	0.725	1.5	1.5	1.08	0.53	1.73	92.2	121.9
	1.5	3.0	3.0	1.31	0.45	1.02	78.3	113.0
NMSSM+	1.5	1.5	3.0	1.29	0.51	1.05	88.5	118.5
	1.5	3.0	1.5	1.32	0.35	1.01	61.3	105.0
	1.5	1.5	1.5	1.30	0.43	1.03	74.2	111.0

see [39]). The term $\mu(H_dH_u)$ in the superpotential is then replaced by the coupling term λSH_dH_u. As in the E_6 inspired SUSY models discussed above, the superfield S acquires a nonzero VEV ($\langle S\rangle = s/\sqrt{2}$), and an effective μ term ($\mu_{\rm eff} = \lambda s/\sqrt{2}$) is automatically generated. However, the simplest model of this type possesses an extended global $SU(2) \times [U(1)]^2$ symmetry[7] that after its breakdown leads to the appearance of the massless CP-odd scalar particle in the Higgs boson spectrum which is a Peccei-Quinn axion [40]. The common way to avoid the axion is to introduce a term cubic in the new singlet superfield $\frac{\kappa}{3}S^3$ in the superpotential that explicitly breaks an additional $U(1)$ global symmetry. Here, to simplify our analysis of the RG flow of the Yukawa couplings, we assume that κ is negligibly small, while the extended global $SU(2) \times [U(1)]^2$ symmetry is explicitly broken by some other mechanism like in some modifications of the NMSSM [38].

The approximate analytical expression (27) can be used for the calculation of the upper bound on the lightest Higgs mass m_{h_1} in the NMSSM and its modifications if we set $g_1' = 0$. From Eq. (27), it follows that for large λ, i.e. $\lambda > \sqrt{2}M_Z/v \simeq 0.52$, the theoretical restriction on m_{h_1} attains its maximal value for $\tan\beta \sim 1$, which is larger than the upper bound on the mass of the lightest Higgs boson in the MSSM. As a consequence, for large low-energy values of λ, the fine-tuning of the MSSM, which is needed to ensure that this model is consistent with the 125–126 GeV SM-like Higgs boson, can be ameliorated within the NMSSM [41]. However, in the NMSSM $\lambda(M_Z) \simeq 0.7$ is the largest value in order not to spoil the validity of the perturbation theory up to the scale M_X. The inclusion of extra $5 + \bar{5}$-plets of matter enlarges the allowed range of λ at low energies [12]. In this context we also explore here the RG flow of the Yukawa couplings within the NMSSM with three families of $5 + \bar{5}$-plets of extra matter (NMSSM+) [42,43] assuming again that the coupling κ is so small that it can be ignored in the leading approximation.

The results of our numerical analysis of the two-loop RG flow of the Yukawa couplings are presented in Figs. 2(c) and 2(d) as well as in Table V. The complete set of the two-loop RG equations that describe the running of the gauge and Yukawa couplings from $Q = M_X$ to the EW scale within the NMSSM and NMSSM+ can be found in [42]. In the case of the NMSSM we set $g_0 = 0.725$, whereas for the analysis of the RG flow of $h_t(Q)$ and $\lambda(Q)$ within the NMSSM+ we fix $g_0 = 1.5$. These values of g_0 lead to $g_i(M_Z)$ which are very close to the experimentally measured values of the SM gauge couplings at the EW scale. Figures 2(c) and 2(d) demonstrate that different trajectories associated with different solutions of the two-loop RG equations tend to get attracted to the invariant line, that corresponds to $\rho_\lambda \simeq \rho_t$ at high energies, and focused in a relatively narrow region at low energies. In the (ρ_t, ρ_λ) plane the intersection points of the invariant and quasifixed line have the following coordinates:

$$\begin{aligned} &\text{(C)}\rho_t = 0.80, \qquad \rho_\lambda = 0.19; \\ &\text{(D)}\rho_t = 1.15, \qquad \rho_\lambda = 0.14 \end{aligned} \tag{28}$$

in the cases of the NMSSM and NMSSM+, respectively.

Naively, one can expect that the inclusion of extra $5 + \bar{5}$-plets of matter should lead to the larger values of the Yukawa couplings at low energies. Indeed, as was mentioned before, extra multiplets of matter change the running of the SM gauge couplings so that their values at the intermediate scale rise when the number of new supermultiplets increases. Since $g_i(Q)$ occurs in the right-hand side of the RG equations with a negative sign, the growth of the gauge couplings prevents the appearance of the Landau pole in the evolution of the Yukawa couplings. It means that in the NMSSM+ $\lambda(M_Z)$ and $h_t(M_Z)$ are allowed to be larger than in the NMSSM, so that the lightest Higgs boson

[7]In the MSSM this global symmetry of the Lagrangian reduces to the gauge one because of the μ term in the superpotential.

in the NMSSM+ can be heavier than in the NMSSM and MSSM. On the other hand, the results presented in Table V and the coordinates of the quasifixed points (28) indicate that the values of $\lambda(M_Z)$ near quasifixed point (D) tend to be smaller than in the vicinity of quasifixed point (C). Thus, for a fixed set of the Yukawa couplings at the GUT scale, the theoretical restrictions on the mass of the SM-like Higgs boson become even more stringent after the inclusion of exotic supermultiplets of matter (see Table V). This happens because $h_t(Q)$ renormalizes by means of strong interactions while $\lambda(Q)$ does not. Because of this, the top-quark Yukawa coupling rises significantly (see Table V) resulting in the decreasing of $\lambda(Q)$ which prevails the growth of this coupling caused by the larger values of $g_i(Q)$. While the increase of the top-quark Yukawa coupling at the EW scale leads to the decreasing of $\tan\beta$, that pushes the lightest Higgs boson mass up, the decreasing of $\lambda(M_Z)$ reduces the upper limit on m_{h_1}. The results of the numerical analysis collected in Table V show that for a fixed set of $h_t(M_X)$ and $\lambda(M_X)$ the last effect dominates. As a consequence, the upper bound on m_{h_1} in the vicinity of quasifixed point (D) tend to be substantially smaller than 125 GeV, so that the corresponding quasifixed point scenario in the NMSSM+ is basically ruled out. In the NMSSM near quasifixed point (C) the low-energy values of the top-quark Yukawa coupling are smaller, while $\lambda(M_Z)$ and $\tan\beta$ are larger than the ones that correspond to the quasifixed point scenarios (A), (B), and (D). As a result, it seems to be possible to find in the vicinity of quasifixed point (C) phenomenologically acceptable solutions with a 125–126 GeV SM-like Higgs boson.

As in quasifixed point scenarios (A) and (B), the relative variations of $h_t(M_Z)$ near quasifixed points (C) and (D) are quite small, i.e. about 4% and 1%, respectively, when $h_t(M_X)$ and $\lambda(M_X)$ vary from 1.5 to 3 (see Table V). As before, the relative deviations of $\lambda(M_Z)$ can be substantially larger, i.e. about 10%–20% for the same interval of variations of $h_t(M_X)$ and $\lambda(M_X)$. Moreover, the values of the gauge and Yukawa couplings as well as $\tan\beta$ associated with quasifixed points (A) and (D) are rather close. At the same time, the upper bound on m_{h_1} in the E_6 inspired SUSY model with extra $U(1)_N$ gauge symmetry is considerably larger than in the NMSSM with three extra pairs of $5+\bar{5}$ supermultiplets of matter because of the $U(1)_N$ D-term contribution to m_{h_1} that increases the two-loop theoretical restriction on m_{h_1} by ∼7–8 GeV. Thus, this relatively small contribution to the lightest Higgs mass plays an important role, enabling us to find phenomenologically acceptable solutions with a 125–126 GeV Higgs mass near quasifixed point (A) in the case of scenario A.

IV. CONCLUSIONS

In this paper, we have explored the RG flow of the gauge and Yukawa couplings within the E_6 inspired SUSY models with extra $U(1)_N$ gauge symmetry under which right-handed neutrinos have zero charge. In these models, single discrete $\tilde{Z}_2^H$ symmetry forbids the tree-level flavor-changing transitions and the most dangerous baryon and lepton number violating operators. Just below the GUT scale, the matter content of these SUSY models includes three copies of 27_i-plets and a set of M_l and $\bar{M}_l$ supermultiplets from the incomplete $27'_l$ and $\overline{27'}_l$ representations of E_6. All supermultiplets M_l are even under the $\tilde{Z}_2^H$ symmetry, whereas all matter superfields, that fill in complete 27_i-plets, are odd. The supermultiplets $\bar{M}_l$ can be either odd or even under the $\tilde{Z}_2^H$ symmetry. In particular, the set of supermultiplets M_l include either lepton $SU(2)_W$ doublet L_4 (scenario A) or color triplet down-type quark d_4^c (scenario B) states to render the lightest exotic quark unstable. In scenario A the exotic quarks are leptoquarks, while scenario B implies that the exotic quarks are diquarks.

Our numerical analysis revealed that the solutions of the two-loop RG equations for the $SU(2)_W$ and $U(1)_Y$ gauge couplings are focused in the infrared region near the quasifixed points which are rather close to the measured values of these couplings at the EW scale. On the other hand, the convergence of the solutions for the strong gauge coupling $g_3(Q)$ to the fixed point is rather weak, because the corresponding one-loop beta function vanishes in scenario A and remains quite small, i.e. $\beta_3 = 1$, in scenario B. Nonetheless, we demonstrated that in the case of scenario A the values of the overall gauge coupling g_0 around 1.5 lead to $g_i(M_Z)$ which are quite close to the measured central values of these couplings at the EW scale including the strong gauge coupling. In scenario B the low-energy values of $g_3(Q)$ are always substantially smaller than the experimentally measured central value of this coupling. It means that the values of $\alpha_3(M_Z)$, which are reasonably close to its measured value, result in the appearance of the Landau pole below the GUT scale, spoiling the gauge coupling unification in this scenario.

Moreover, our analysis indicates that in this case the SM-like Higgs state tends to be lighter than 125 GeV. Indeed, we argued that the solutions of the two-loop RG equations for the Yukawa couplings are concentrated near the quasifixed points when $h_t(M_X)$ and $\lambda(M_X)$ grow. In scenarios A and B, these quasifixed points correspond to the values of $\tan\beta$ around 1 and 1.2, respectively. Near the quasifixed point, the low-energy values of the coupling λ tend to be slightly larger in scenario A than in scenario B. As a consequence, in the vicinity of the quasifixed point the lightest Higgs state is allowed to be a few GeV heavier in scenario A than in scenario B. Our estimations show that for $1.5 \lesssim h_t(M_X), \lambda(M_X) \lesssim 3$ the maximal value of the lightest Higgs mass is just above 126 GeV in scenario A and a few GeV lower than 125 GeV in scenario B. Thus it seems to be rather problematic to find phenomenologically acceptable solutions near the quasifixed point in the case of scenario B.

In this context it is worth noting that the absolute maximum value of the lightest Higgs mass in the E_6 inspired SUSY models with extra $U(1)_N$ symmetry is about 155 GeV [3], so that it is considerably larger than the upper bounds on m_{h_1} in the vicinity of the quasifixed points. This absolute maximum value of m_{h_1} is attained for $\tan\beta \simeq$ 1.5–2 that correspond to the substantially lower values of $h_t(M_Z)$ than the ones associated with the quasifixed point scenarios. Since larger values of the top-quark Yukawa coupling result in smaller $\lambda(M_Z)$, the two-loop upper bounds on m_{h_1} near the quasifixed points are significantly lower than 155 GeV. Besides, the solutions with a 125–126 GeV SM-like Higgs boson can be obtained only if $\lambda(M_Z) > g_1'(M_Z)$. Such solutions can be found in the vicinity of the quasifixed point in the case of scenario A. However, for $\lambda(M_Z) > g_1'(M_Z)$ the Higgs spectrum has very hierarchical structure, which implies that all Higgs states except the lightest one cannot be discovered at the LHC and the phenomenologically viable solutions associated with the quasifixed point scenarios are very fine-tuned.

Finally, we compared the results of our analysis of the quasifixed point scenarios in the E_6 inspired SUSY models with the corresponding results in the NMSSM and NMSSM+. The two-loop RG flow of the Yukawa couplings within the NMSSM+ is very similar to the one in scenario A. The low-energy values of the Yukawa couplings and $\tan\beta$ associated with the quasifixed point scenarios are very close in both models as well. Nevertheless, because of the $U(1)_N$ D-term contribution to m_{h_1}, the upper bound on the lightest Higgs boson mass is larger in scenario A as compared with the NMSSM+. As a result, in the NMSSM+ the theoretical restriction on m_{h_1} in the vicinity of the quasifixed point is lower than 120 GeV. This does not rule out NMSSM+ but definitely disfavors the corresponding scenario. In the NMSSM, the top-quark Yukawa coupling is smaller, whereas $\lambda(M_Z)$ and $\tan\beta$ are larger near the quasifixed point as compared with the quasifixed point scenarios in the E_6 inspired SUSY models discussed here and NMSSM+. Therefore, the upper bound on the mass of the lightest Higgs boson is less stringent and can be almost as large as 130 GeV.

The results presented in this article show that it is not so easy to get 125–126 GeV SM-like Higgs mass within the nonminimal SUSY models mentioned above as one could naively expect. In this context, it would be appropriate to recall that in the MSSM large loop corrections are required to raise the Higgs boson mass to 125 GeV. This can be achieved only if top squarks are relatively heavy that leads to some degree of fine-tuning. As follows from Tables 4 and 5, near the quasifixed points in the case of scenario A and NMSSM the tree-level upper bound on the lightest Higgs boson mass may be still 10 GeV larger than in the MSSM, so that in order to match the 125–126 GeV Higgs mass value the size of loop corrections can be smaller and top squarks can be lighter in these cases as compared with the ones in the minimal SUSY model.

ACKNOWLEDGMENTS

We thank P. Athron, A. V. Borisov, S. F. King, S. Pakvasa, O. Pavlovsky, A. Thomas, X. Tata, M. Trusov, and A. Williams for fruitful discussions. R. N. is also grateful to E. Boos, M. Dubinin, S. Demidov, D. Gorbunov, M. Libanov, V. Novikov, O. Kancheli, D. Kazakov, V. Rubakov, M. Shifman, S. Troitsky, and M. Vysotsky for valuable comments and remarks. This work was supported by the University of Adelaide and the Australian Research Council through the ARC Centre of Excellence for Particle Physics at the Terascale (CoEPP).

[1] G. Aad *et al.* (ATLAS Collaboration), Phys. Lett. B **716**, 1 (2012); (ATLAS Collaboration), Report No. ATLAS-CONF-2012-162.

[2] S. Chatrchyan *et al.* (CMS Collaboration), Phys. Lett. B **716**, 30 (2012); S. Chatrchyan *et al.* (CMS Collaboration), Report No. CMS-PAS-HIG-12-045.

[3] S. F. King, S. Moretti, and R. Nevzorov, Phys. Rev. D **73**, 035009 (2006).

[4] S. F. King, S. Moretti, and R. Nevzorov, Phys. Lett. B **634**, 278 (2006).

[5] T. Hambye, E. Ma, M. Raidal, and U. Sarkar, Phys. Lett. B **512**, 373 (2001); S. F. King, R. Luo, D. J. Miller, and R. Nevzorov, J. High Energy Phys. 12 (2008) 042.

[6] S. F. King, S. Moretti, and R. Nevzorov, arXiv:hep-ph/0601269; S. F. King, S. Moretti, and R. Nevzorov, Report No. CERN-2006-009, edited by S. Kraml *et al.* [arXiv:hep-ph/0608079]; S. F. King, S. Moretti, and R. Nevzorov, AIP Conf. Proc. **881**, 138 (2007); R. Howl and S. F. King, J. High Energy Phys. 01 (2008) 030; J. P. Hall, S. F. King, R. Nevzorov, S. Pakvasa, and M. Sher, Phys. Rev. D **83**, 075013 (2011); P. Athron, J. P. Hall, R. Howl, S. F. King, D. J. Miller, S. Moretti, and R. Nevzorov, Nucl. Phys. B, Proc. Suppl. **200–202**, 120 (2010); R. Nevzorov and S. Pakvasa, Phys. Lett. B **728**, 210 (2014).

[7] P. Athron, S. F. King, D. J. Miller, S. Moretti, and R. Nevzorov, arXiv:0810.0617; Phys. Lett. B **681**, 448 (2009); Phys. Rev. D **80**, 035009 (2009); **84**, 055006 (2011); **86**, 095003 (2012).

[8] P. Athron, D. Stockinger, and A. Voigt, Phys. Rev. D **86**, 095012 (2012).

[9] M. Sperling, D. Stckinger, and A. Voigt, J. High Energy Phys. 07 (2013) 132.

[10] R. Nevzorov, Phys. Rev. D **87**, 015029 (2013).

[11] U. Ellwanger and C. Hugonie, Mod. Phys. Lett. A **22**, 1581 (2007).

[12] M. Masip, R. Munoz-Tapia, and A. Pomarol, Phys. Rev. D **57**, R5340 (1998).

[13] J. Rich, M. Spiro, and J. Lloyd-Owen, Phys. Rep. **151**, 239 (1987); P. F. Smith, Contemp. Phys. **29**, 159 (1988); T. K. Hemmick *et al.*, Phys. Rev. D **41**, 2074 (1990).

[14] G. F. Giudice and A. Masiero, Phys. Lett. B **206**, 480 (1988); J. A. Casas and C. Muñoz, Phys. Lett. B **306**, 288 (1993).

[15] S. F. King, S. Moretti, and R. Nevzorov, Phys. Lett. B **650**, 57 (2007).

[16] S. Hesselbach, D. J. Miller, G. Moortgat-Pick, R. Nevzorov, and M. Trusov, Phys. Lett. B **662**, 199 (2008); S. Hesselbach, D. J. Miller, G. Moortgat-Pick, R. Nevzorov, and M. Trusov, arXiv:0710.2550; S. Hesselbach, G. Moortgat-Pick, D. J. Miller, R. Nevzorov, and M. Trusov, arXiv:0810.0511.

[17] J. P. Hall, S. F. King, R. Nevzorov, S. Pakvasa, and M. Sher, Phys. Rev. D **83**, 075013 (2011); *Proc. Sci., QFTHEP2010* (2010), p. 069; J. P. Hall, S. F. King, R. Nevzorov, S. Pakvasa, and M. Sher, arXiv:1109.4972.

[18] J. P. Hall and S. F. King, J. High Energy Phys. 08 (2009) 088.

[19] J. M. Frere, R. B. Nevzorov, and M. I. Vysotsky, Phys. Lett. B **394**, 127 (1997).

[20] J. A. Casas, J. R. Espinosa, and H. E. Haber, Nucl. Phys. **B526**, 3 (1998); G. K. Yeghiyan, M. Jurčišin, and D. I. Kazakov, Mod. Phys. Lett. A **14**, 601 (1999); S. Codoban, M. Jurčišin, and D. Kazakov, arXiv:hep-ph/9912504.

[21] B. Brahmachari, Mod. Phys. Lett. A **12**, 1969 (1997).

[22] J. Beringer *et al.* (Particle Data Group), Phys. Rev. D **86**, 010001 (2012).

[23] K. S. Babu, C. Kolda, and J. March-Russell, Phys. Rev. D **54**, 4635 (1996).

[24] P. Langacker and J. Wang, Phys. Rev. D **58**, 115010 (1998); D. Suematsu, Phys. Rev. D **59**, 055017 (1999).

[25] B. Schrempp and F. Schrempp, Phys. Lett. B **299**, 321 (1993); B. Schrempp, Phys. Lett. B **344**, 193 (1995); B. Schrempp and M. Wimmer, Prog. Part. Nucl. Phys. **37**, 1 (1996).

[26] R. B. Nevzorov and M. A. Trusov, Yad. Fiz. **64**, 1375 (2001) [Phys. At. Nucl. **64**, 1299 (2001)]; Yad. Fiz. **65**, 359 (2002) [Phys. At. Nucl. **65**, 335 (2002)]; R. B. Nevzorov, K. A. Ter-Martirosyan, and M. A. Trusov, arXiv:hep-ph/0301068.

[27] R. Tarrach, Nucl. Phys. **B183**, 384 (1981); N. Gray, D. J. Broadhurst, W. Grafe, and K. Schilcher, Z. Phys. C **48**, 673 (1990); D. J. Broadhurst, N. Gray, and K. Schilcher, Z. Phys. C **52**, 111 (1991); K. G. Chetyrkin and M. Steinhauser, Phys. Rev. Lett. **83**, 4001 (1999); Nucl. Phys. **B573**, 617 (2000).

[28] M. Carena, M. Quiros, and C. E. M. Wagner, Nucl. Phys. **B461**, 407 (1996).

[29] U. Ellwanger and C. Hugonie, Eur. Phys. J. C **25**, 297 (2002).

[30] K. Inoue, A. Kakuto, H. Komatsu, and S. Takeshita, Prog. Theor. Phys. **67**, 1889 (1982); R. Flores and M. Sher, Ann. Phys. (N.Y.) **148**, 95 (1983).

[31] A. Djouadi, Phys. Rep. **459**, 1 (2008).

[32] A. Djouadi, J.-L. Kneur, and G. Moultaka, Comput. Phys. Commun. **176**, 426 (2007).

[33] S. Heinemeyer, W. Hollik, and G. Weiglein, Comput. Phys. Commun. **124**, 76 (2000); Eur. Phys. J. C **9**, 343 (1999); G. Degrassi, S. Heinemeyer, W. Hollik, P. Slavich, and G. Weiglein, Eur. Phys. J. C **28**, 133 (2003); M. Frank, T. Hahn, S. Heinemeyer, W. Hollik, H. Rzehak, and G. Weiglein, J. High Energy Phys. 02 (2007) 047.

[34] D. J. Miller, S. Moretti, and R. Nevzorov, in *Proceedings of the Eighteenth International Workshop on High-Energy Physics and Quantum Field Theory (QFTHEP 2004)*, edited by M. N. Dubinin and V. I. Savrin (Moscow State University, Moscow, 2004), p. 212; D. J. Miller, S. Moretti, and R. Nevzorov, arXiv:hep-ph/0501139.

[35] D. J. Miller, R. Nevzorov, and P. M. Zerwas, Nucl. Phys. **B681**, 3 (2004); R. Nevzorov and D. J. Miller, in *Proceedings of the Seventh Workshop "What Comes beyond the Standard Model,"* edited by N. S. Mankoc-Borstnik, H. B. Nielsen, C. D. Froggatt, and D. Lukman (DMFA-Zaloznistvo, Ljubljana, 2004), p. 107; R. Nevzorov and D. J. Miller, arXiv:hep-ph/0411275.

[36] P. A. Kovalenko, R. B. Nevzorov, and K. A. Ter-Martirosian, Yad. Fiz. **61**, 898 (1998) [Phys. At. Nucl. **61**, 812 (1998)]; R. B. Nevzorov and M. A. Trusov, Zh. Eksp. Teor. Fiz. **91**, 1251 (2000) [J. Exp. Theor. Phys. **91**, 1079 (2000)]; R. B. Nevzorov, K. A. Ter-Martirosyan, and M. A. Trusov, Yad. Fiz. **65**, 311 (2002) [Phys. At. Nucl. **65**, 285 (2002)].

[37] P. Fayet, Nucl. Phys. **B90**, 104 (1975); P. Fayet, Phys. Lett. **64B**, 159 (1976); **69B**, 489 (1977); **84B**, 416 (1979); H. P. Nilles, M. Srednicki, and D. Wyler, Phys. Lett. **120B**, 346 (1983); J. M. Frere, D. R. Jones, and S. Raby, Nucl. Phys. **B222**, 11 (1983); J. P. Derendinger and C. A. Savoy, Nucl. Phys. **B237**, 307 (1984); A. I. Veselov, M. I. Vysotsky, and K. A. Ter-Martirosian, Sov. Phys. JETP **63**, 489 (1986); J. R. Ellis, J. F. Gunion, H. E. Haber, L. Roszkowski, and F. Zwirner, Phys. Rev. D **39**, 844 (1989); L. Drees, Int. J. Mod. Phys. A **04**, 3635 (1989); L. Durand and J. L. Lopez, Phys. Lett. B **217**, 463 (1989); U. Ellwanger, M. Rausch de Traubenberg, and C. A. Savoy, Phys. Lett. B **315**, 331 (1993); U. Ellwanger, M. Rausch de Traubenberg, and C. A. Savoy, Z. Phys. C **67**, 665 (1995); U. Ellwanger, M. Rausch de Traubenberg, and C. A. Savoy, Nucl. Phys. **B492**, 307 (1997); U. Ellwanger, Phys. Lett. B **303**, 271 (1993); P. Pandita, Z. Phys. C **59**, 575 (1993); T. Elliott, S. F. King, and P. L. White, Phys. Rev. D **49**, 2435 (1994); T. Elliott, S. F. King, and P. L. White, Phys. Rev. D **52**, 4183 (1995); F. Franke and H. Fraas, Int. J. Mod. Phys. A **12**, 479 (1997).

[38] C. Panagiotakopoulos and K. Tamvakis, Phys. Lett. B **446**, 224 (1999); **469**, 145 (1999); C. Panagiotakopoulos and A. Pilaftsis, Phys. Rev. D **63**, 055003 (2001); A. Dedes, C. Hugonie, S. Moretti, and K. Tamvakis, Phys. Rev. D **63**, 055009 (2001); A. Menon, D. E. Morrissey, and C. E. M. Wagner, Phys. Rev. D **70**, 035005 (2004); C. Balazs, M. S. Carena, A. Freitas, and C. E. M. Wagner, J. High Energy Phys. 06 (2007) 066.

[39] U. Ellwanger, C. Hugonie, and A. M. Teixeira, Phys. Rep. **496**, 1 (2010); U. Ellwanger, Eur. Phys. J. C **71**, 1782 (2011).

[40] S. Weinberg, Phys. Rev. Lett. **40**, 223 (1978); F. Wilczek, Phys. Rev. Lett. **40**, 279 (1978).

[41] M. Bastero-Gil, C. Hugonie, S. F. King, D. P. Roy, and S. Vempati, Phys. Lett. B **489**, 359 (2000); A. Delgado, C. Kolda, J. P. Olson, and A. de la Puente, Phys. Rev. Lett. **105**, 091802 (2010); U. Ellwanger, G. Espitalier-Noel, and C. Hugonie, J. High Energy Phys. 09 (2011) 105; L. J. Hall, D. Pinner, and J. T. Ruderman, J. High Energy Phys. 04 (2012) 131; K. Agashe, Y. Cui, and R. Franceschini, J. High Energy Phys. 02 (2013) 031.G. G. Ross and K. Schmidt-Hoberg, Nucl. Phys. **B862**, 710 (2012); M. Perelstein and B. Shakya, Phys. Rev. D **88**, 075003 (2013)

[42] S. F. King, M. Muhlleitner, and R. Nevzorov, Nucl. Phys. **B860**, 207 (2012).

[43] J. P. Hall and S. F. King, J. High Energy Phys. 01 (2013) 076; S. F. King, M. Mhlleitner, R. Nevzorov, and K. Walz, Nucl. Phys. **B870**, 323 (2013).